Clinical Evaluation of Carbon-11-Phenylephrine: MAO-Sensitive Marker of Cardiac Sympathetic Neurons

David M. Raffel, James R. Corbett, Renato B. del Rosario, David L. Gildersleeve, Ping-Chun Chiao, Markus Schwaiger and Donald M. Wieland

Division of Nuclear Medicine, Department of Internal Medicine, University of Michigan Medical School, Ann Arbor, Michigan; Department of Nuclear Medicine, Technical University of Münich, Münich, Germany

The sympathomimetic drug phenylephrine recently has been labeled with ^{11}C for use in PET studies of cardiac sympathetic innervation. Previous reports using isolated perfused rat heart models indicate that phenylephrine is metabolized by intraneuronal monoamine oxidase (MAO). This report compares the imaging characteristics, neuronal selectivity and kinetics of (−)-[^{11}C]phenylephrine (PHEN) to the structurally similar but MAO-resistant analog (−)-[^{11}C]-*meta*-hydroxyephedrine (HED), an established heart neuronal marker. **Methods:** Fourteen healthy volunteers were studied with PET and PHEN. Ten had paired studies with HED; four of the 10 were scanned a second time with each tracer after oral administration of desipramine, a selective neuronal transport blocker. Hemodynamic and electrocardiographic responses were monitored. Blood levels of intact radiotracer and radiolabeled metabolites were determined from venous blood samples taken during the PET study. Myocardial retention indices for both tracers were calculated. **Results:** No hemodynamic or electrocardiographic effects were observed with either tracer. PHEN showed reduced myocardial retention at 50 min compared to HED; however, image quality and uniformity of distribution were comparable. PHEN cleared from myocardium with a mean half-time of 59 ± 5 min, while myocardial levels of HED remained constant. PHEN metabolites appeared in the blood approximately three times faster than HED metabolites. Desipramine pretreatment markedly reduced (>60%) myocardial retention of both PHEN and HED. **Conclusion:** PHEN provides PET images of human heart comparable in quality and uniformity to HED. Like HED, PHEN localizes in the sympathetic nerves of the heart. However, the more rapid efflux of PHEN, that is likely mediated by MAO, may provide information on the functional status of cardiac sympathetic neurons unobtainable with HED.

Key Words: sympathetic nervous system; PET; carbon-11-phenylephrine; carbon-11-hydroxyephedrine; norepinephrine transporter

J Nucl Med 1996; 37:1923–1931

We have reported the use of (−)-[^{11}C]-*meta*-hydroxyephedrine (HED) and PET to assess sympathetic nerve viability of the heart in animal models and in humans (*1–4*). Normal volunteers (*4*) and patients with myocardial infarction (*5*), diabetes mellitus (*6*), congestive heart failure (*7*), cardiac transplantation (*8*) and life-threatening arrhythmias (*7, 9*) have been studied with this neuronal mapping agent.

The structural similarity of HED to the endogenous neurotransmitter norepinephrine enables it to enter sympathetic neurons by the neuronal norepinephrine transporter (uptake$_1$), where it is transported into storage vesicles by the vesicular monoamine transporter (*1, 2, 10*). However, unlike norepinephrine, HED is not a substrate for monoamine oxidase (MAO). Removal of the α-methyl group from HED provides a tracer that retains high neuronal affinity but is metabolized by neuronal MAO. This α-normethyl analog of HED is the common nasal decongestant phenylephrine. The synthesis and preliminary evaluation of (−)-[^{11}C]phenylephrine (PHEN) in animals have been reported recently (*11–14*). These preliminary studies have established that PHEN localizes in cardiac sympathetic nerve varicosities and that subsequent release of radioactivity from the heart reflects degradation of PHEN by neuronal MAO. Because of its susceptibility to neuronal oxidation by MAO, PHEN potentially can provide insight into several aspects of neuronal function, including the status of the neuronal and vesicular norepinephrine transporters, as well as the oxidative robustness of the neuron. We report here the tandem evaluation of PHEN and HED in normal volunteers.

MATERIALS AND METHODS

Subjects

Fourteen healthy volunteers (10 women, 4 men) 33.6 ± 10.6 yr of age (range 22–56 yr) were studied. On the basis of age, gender, asymptomatic status and normal resting ECG, all volunteers had a low likelihood of having hemodynamically important coronary heart disease or prior myocardial infarction, and none of the subjects had any evidence of diabetes mellitus or hypertension. None of the volunteers were taking medications known to interfere with neuronal uptake of norepinephrine (*15*), including tricyclic antidepressants and amiodarone. Other noncardiac medications (specifically birth control medications, n = 10) were continued as usual. None of the volunteers were hypertensive and there were no significant differences in heart rate or blood pressure at the times of the PHEN and HED studies.

Synthesis of Carbon-11-(−)-Phenylephrine

The chemical structures of norepinephrine, HED and PHEN are shown in Figure 1. The radiochemical synthesis of [^{11}C]PHEN has recently been described by this laboratory (*11*). PHEN (>18.5 TBq/mmol (500 Ci/mmol) 30–60% radiochemical yield, EOS) was routinely synthesized by direct methylation of (1*R*)-*m*-octopamine (*12*) with [^{11}C]methyl triflate (*16, 17*) and purified by cation-exchange HPLC (>95% radiochemical purity). For clinical studies, the product was formulated in 0.9% saline containing 0.02 *M* monobasic sodium phosphate.

Cardiac PET Studies

The study protocol was approved by the Institutional Review Board of the University of Michigan Medical Center, and all volunteers gave written informed consent before participation. All 14 volunteers were studied with PHEN. Ten of the 14 had a paired HED study. For those subjects who were imaged with both tracers, the PHEN and HED PET studies were done consecutively on the

Received Dec. 7, 1995; revision accepted Apr. 10, 1996.

For correspondence or reprints contact: David M. Raffel, PhD, Cyclotron/PET Facility, 3480 Kresge III Bldg., University of Michigan, Ann Arbor, MI 48109-0552.

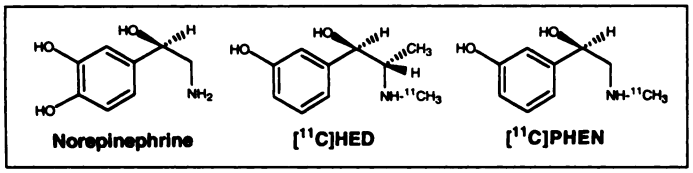

FIGURE 1. Chemical structures of norepinephrine, [^{11}C]HED and [^{11}C]PHEN.

same day. All studies were performed at rest without exercise or pharmacological stress.

PET imaging studies were performed with a 15-slice whole-body tomograph (Siemens/CTI ECAT 931/08-12). After placing a 22-gauge intravenous cannula in an antecubital vein and positioning the subject in the tomograph with the aid of an [^{13}N]ammonia scout image, a 15-min transmission scan was acquired using a retractable ^{68}Ge ring source for subsequent attenuation correction of the emission data. Data acquisition was started as approximately 740 MBq (20 mCi) of PHEN were intravenously administered as a bolus injection. The imaging sequence consisted of a 1-hr dynamic acquisition comprised of 23 frames (framing rates 12 × 10 sec, 2 × 30 sec, 2 × 60 sec, 2 × 150 sec, 2 × 300 sec, 2 × 600 sec, 1 × 1200 sec). For the HED study, the same imaging protocol was used after injection of approximately 740 MBq (20 mCi) of HED. A delay of at least 60 min between the end of the PHEN study and the start of the HED study was imposed to allow myocardial ^{11}C activity to clear and decay to negligible levels. Blood samples (3 ml each) were drawn at 1, 5, 10, 20, 40 and 60 min after radiotracer injection for the determination of radiolabeled metabolites in blood.

Desipramine Studies

Four of the 10 volunteers who had paired PHEN and HED studies were scanned a second time after desipramine treatment. Each volunteer took 50 mg desipramine orally 10–12 hr before and again 1 hr before the repeat PHEN and HED studies. These comparative studies after desipramine were performed within 5 days of the initial PET imaging studies.

Image Reconstruction

The HED and PHEN emission data were attenuation corrected and reconstructed using filtered backprojection (Hanning filter with a cutoff of 0.3 cycles/pixel). Transaxial reconstructed images were transferred to a SUN workstation (SUN Microsystems, Mountain View, CA) where they were formatted into three-dimensional volume data and resliced into 12 short-axis sections from apex to base of the left ventricle, as well as multiple vertical and horizontal long-axis sections. Static short-axis images of the data acquired 40–60 min postinjection were taken from the dynamic acquisition sequences for visual interpretation.

Polar Map Generation

Polar maps were constructed from eight contiguous planes of the 12-plane short-axis dataset. The apical-most plane was selected visually as the first plane in which the myocardial activity resembled a solid disk, and for which the next seven more basal planes all demonstrated the characteristic donut shape of myocardial activity seen in short-axis images of the left ventricle. A modified version of a previously described circumferential profile, maximum search algorithm (*18*) was used to generate the polar maps. The modified algorithm processes each short-axis left ventricular slice into major and minor sectors. Major sectors are established by using the circumferential profile, maximum search scheme to identify large arcs of myocardial tissue automatically; each of these major sectors is then equally divided into a specified number of minor sectors. This approach is particularly useful in patients with large defects in radiotracer retention because it allows the search algorithm to effectively bridge gaps in the contour of myocardial activity. For this study, the eight selected short-axis images were each sectioned into 60 total sectors, typically using four major sectors and 15 minor sectors. Time-activity curves were determined for each sector and stored for later analyses, including construction of polar maps of radiotracer retention.

Homogeneity of Relative Myocardial Tracer Retention

The homogeneity of radiotracer retention in the normal left ventricle was assessed using polar maps of relative tissue ^{11}C concentrations generated from the final frame of the time-activity data (40–60 min post-tracer injection). Relative tissue concentrations were calculated by dividing the activity in each sector by the maximum activity in the map. These values were then averaged in several myocardial regions to assess the uniformity of radiotracer uptake throughout the left ventricle. Apical values represent the average of all sectors in the two most apical planes. Distal values for anterior, septal, inferior and lateral segments were obtained by averaging the appropriate sectors in the three planes adjacent to the two apical planes. Similarly, proximal averages for the anterior, septal, inferior and lateral segments were obtained from the next three planes adjacent to the distal planes.

Blood Metabolite Studies

A modification of our previously reported solid-phase extraction method for the separation of ^{11}C-labeled metabolites of HED (*1*) was used to measure the amounts of ^{11}C-labeled metabolites and intact ^{11}C-labeled tracer in blood samples obtained during both the PHEN and the HED studies. When using the previously reported method, we observed excessive variability in the recovery of [^{11}C]HED from whole blood. Furthermore, when we attempted to apply the method to [^{11}C]PHEN, low recoveries of intact tracer from protein-free extracts were obtained. On closer examination of the method, we found that the retention of [^{11}C]HED and [^{11}C]PHEN by the C-18 Sep-Pak (Waters, Milford, MA) depends not only on sample pH (optimum pH 7.2–8.0), but also on the ionic strength of the sample matrix. The presence of excess 5-sulfosalicilic acid (5-SSA) after protein precipitation or phosphate buffer >20 m*M* resulted in low recovery of intact tracer. The modifications to the previous method include replacement of the 5-SSA with perchloric acid and removal of excess perchloric acid by precipitation with KOH buffered with K_2HPO_4 (final concentration <20 m*M*) to minimize sample ionic strength. Under the conditions of the assay described below, when a human blood sample is spiked with [^{11}C]HED or [^{11}C]PHEN, more than 95% of the radioactivity extracted into the protein-free supernatant is retained by the Sep-Pak. The current method is as follows. A 1.0-ml aliquot of each blood sample was transferred to a counting vial for measurement of whole-blood radioactivity. A 2.0-ml aliquot of each blood sample was transferred to a 12-ml polypropylene test tube containing 2.0 ml of deionized water and vortexed to lyse red blood cells. Two 1.0-ml aliquots of the lysed sample were drawn; each aliquot was transferred to a 2-ml microfuge tube containing 200 μl of ice-cold 2.0 N $HClO_4$ (final concentration 0.3 N) and vigorously vortexed to deproteinize the samples. After centrifugation for 2 min at 12,000 × g, the protein-free supernatants from both microfuge tubes were transferred to a 12-ml polypropylene test tube containing a neutralization solution (40 μl 1.0 *M* K_2HPO_4 + 450 μl 1.0 N KOH), vortexed and adjusted to pH 7.2–8.0 with 1.0 N KOH, as necessary. The two protein pellets were placed together for gamma counting. The neutralized samples were transferred to a C-18 Sep-Pak (previously activated with 5 ml of methanol and washed with 20 ml of deionized water), and labeled metabolites were eluted from the Sep-Pak with two 10-ml aliquots of deionized water. Finally, the whole-blood sample, the protein pellets, the two metabolite fractions (M_1, M_2) and the Sep-Pak (SP) were counted for radioactivity in a gamma counter.

All radioactivity measurements were decay-corrected to the time of radiotracer injection.

Quantitative Analysis of Blood Metabolite Data

The metabolites fraction (MF) of total blood radioactivity was estimated as the ratio of the activity measured in the two metabolite fractions ($M_1 + M_2$) divided by the total radioactivity transferred to the Sep-Pak ($M_1 + M_2$ + SP) or MF = $(M_1 + M_2)/(M_1 + M_2 +$ SP). The fraction of intact radiotracer (IRF) was estimated as (1.0 − MF). Exponential fitting of the IRF as a function of time was performed to characterize the disappearance of intact radiotracer from the blood.

Retention Index Calculation

To quantify myocardial uptake of PHEN and HED, a retention index approach was adopted (*6*). A retention index can be calculated for any image frame in the dynamic acquisition sequence. If T_1 is the acquisition start time of the image frame and T_2 is the stop time, the retention index for each sector is calculated as:

$$\text{Retention index (ml blood/min/ml tissue)} = \frac{C_t(T_1{:}T_2)}{\int_0^{T_2} C_p(t)dt},$$

where $C_t(T_1{:}T_2)$ is the radiotracer tissue concentration in the sector in the T_1 to T_2 image frame (units: PET counts) and $C_p(t)$ is the arterial blood concentration as a function of time determined from the image data (also in PET counts). Arterial blood activity data were obtained directly from the PET images by placing a region of interest (ROI; 5 by 5 pixels) over the left ventricular chamber in the most basal plane of the 12-plane short-axis data set. The arterial blood data were corrected for metabolites by multiplying the PET counts measured inside the LV chamber ROI by the estimated fraction of intact tracer at the midtime for each image frame. Retention index values were calculated for PHEN and HED using the last two frames of the dynamic dataset, 30–40 min and 40–60 min postinjection. Retention indices were calculated twice: once with the arterial blood data as directly measured from the PET images and the second time with the metabolite-corrected blood data. This was done to investigate the necessity of blood metabolite corrections for the retention index calculation. In both cases, the arterial blood data (with and without metabolite correction) were linearly interpolated to a 1-sec time grid before integration. As previously described for the tracer homogeneity analysis, individual sector retention index values were averaged for apical, distal and proximal LV segments.

For plots of time-activity data, the measured PET counts were converted to units of MBq/ml by multiplying by the PET scanner calibration factor, which has units of MBq/ml/PET count. This calibration factor is determined weekly in our facility by imaging a 20-cm cylindrical flood phantom filled with an aqueous solution of ^{18}F at a known concentration.

PHEN Washout Kinetics Analysis

PHEN clears from the heart quickly enough to allow estimation of a washout half-time. It is not possible to make such a measurement for HED because the myocardial concentration of HED remains constant after initial uptake until the end of the scan. For each sector of the PHEN polar map, the corresponding time-activity data between 6 and 60 min post-tracer injection were fit to a single-exponential decay process. The resultant exponential decay constants were averaged over all sectors in the polar map to estimate a global average washout half-time for each normal volunteer.

Statistical Analysis

Data are expressed as mean ± 1 s.d. Statistical comparisons between measures were made using the two-tailed t-test; a probability value $p < 0.05$ was considered significant. Correlation between the retention indices of PHEN and HED was determined by linear regression analysis using a least squares technique.

RESULTS

Physiological Effects of Carbon-11-PHEN and Carbon-11-HED

None of the volunteers had any symptoms related to the injection of either PHEN or HED. Specifically, there were no pressor effects such as palpitations, chest pain or headache. There were no significant differences between the heart rates, or systolic or diastolic blood pressures recorded during either of the paired studies.

Regional Tracer Distribution

Measures of image quality, including myocardial uptake, heart-to-lung, heart-to-liver and heart-to-blood activity ratios, were generally similar for PHEN and HED. Representative midventricular short-axis images at image frame midtimes of 6, 13, 35 and 50 min post-tracer administration in a normal volunteer are shown in Figure 2. Myocardial concentrations of PHEN and HED are comparable a few minutes after injection, but there is appreciable clearance of PHEN from the myocardium during the 60-min imaging period. In contrast, myocardial levels of HED are constant throughout the study. Representative short-axis, horizontal long-axis and vertical long-axis slices are shown in Figure 3.

The relative regional tracer distributions of PHEN and HED at 40–60 min after injection are shown in Figure 4. The distributions were each relatively homogeneous; for both tracers, however, the retention in the apex was significantly lower than in all other LV regions ($p < 0.004$). Excluding the apical region, there were no significant differences between any of the other eight regions for either PHEN or HED. Likewise, there were no significant differences between PHEN and HED relative tracer distributions in direct region-to-region comparisons.

Blood Metabolites

Analyses of blood metabolites were performed for 12 of the 14 PHEN subjects and 6 of the 10 HED subjects. For PHEN, the intact radiotracer fraction as a function of time was found to be well described by a single-exponential decay process plus a constant background term. HED, on the other hand, required only the single-exponential decay process; no background term was necessary. The results of fitting PHEN and HED blood data to these exponential models are given in Table 1. Metabolites of PHEN appeared in blood almost three times as quickly as HED metabolites ($\lambda = 0.070$ vs. $0.024\ min^{-1}$, respectively). For both PHEN and HED, there were no statistically significant differences in the fitted parameters describing the rate of metabolite formation in blood between the control and desipramine block studies.

Retention Index Values

The average global and regional retention index (RI) values from the 40–60-min image frame are presented in Table 2. Global mean RI values for the 30–40-min image frame were: PHEN: 0.0456 ± 0.0075 using uncorrected blood data; 0.0757 ± 0.0153 using metabolite corrected blood data. HED: 0.103 ± 0.015 using uncorrected blood data; 0.131 ± 0.022 using metabolite corrected blood data. Primarily due to the faster myocardial clearance of PHEN relative to HED, the RI values of PHEN were significantly lower than those of HED.

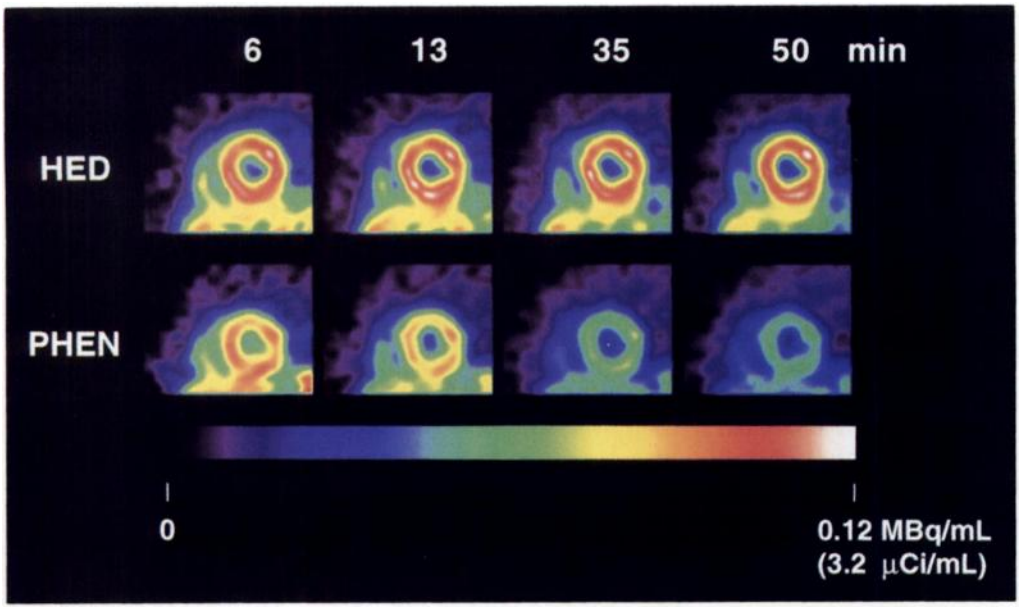

FIGURE 2. Corresponding midventricular short-axis images PHEN and HED from a normal volunteer at image frame mid-times of 6, 13, 35 and 50 min post-tracer injection.

The regional variation of the RI values are, by definition, identical to those reported for the relative homogeneity of tissue tracer activity. Apical regions were significantly lower than all other regions for both PHEN and HED. Correction for blood metabolites resulted in increased RI values because the metabolite correction reduces the denominator in the RI calculation. This effect is more pronounced for PHEN since blood levels of intact PHEN fall more quickly than blood levels of intact HED. Correcting for blood metabolites increased the 40–60-min RI values on average by factors of 2.0 ± 0.2 for PHEN and 1.4 ± 0.1 for HED.

An analysis of the correlation between the calculated RI values of PHEN and HED was performed (Fig. 5). For the six normal volunteers who had both PHEN and HED blood metabolite assays, the RI values of PHEN and HED for each heart territory (apical, proximal septal, etc.) were compared. This was done using the 40–60-min RI values, calculated with and without blood metabolite corrections. When no corrections were made for blood metabolites, the correlation between the regional RI values of PHEN and HED was low, but statistically significant ($p < 0.015$). However, when the RI values were calculated with blood data corrected for metabolites, the correlation was stronger and highly significant ($p < 0.0001$). These results suggest that blood metabolite corrections yield RI values that more accurately reflect the neuronal retention of the tracers.

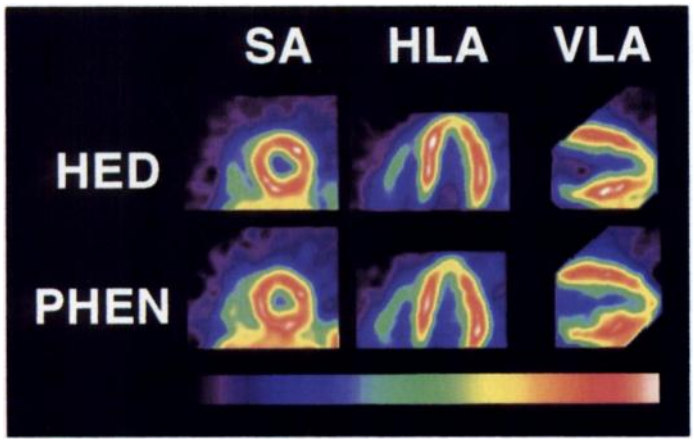

FIGURE 3. Comparison of HED (top) and PHEN (bottom) distributions in a normal volunteer. Corresponding short-axis (SA), horizontal long-axis (HLA) and vertical long-axis (VLA) images from the same normal volunteer as in Figure 2 are shown.

Desipramine Studies

In the four normal volunteers studied after oral administration of desipramine, there was a consistent increase in resting heart rate at the time of the desipramine PET studies from a mean of 65 ± 15 (control) to 83 ± 11 bpm. There were no significant changes in either systolic or diastolic blood pressures after desipramine. Again, there were no changes in either heart rates or blood pressures induced by the administration of either PHEN or HED.

After oral desipramine, there were marked decreases in myocardial levels of radioactivity in both PHEN and HED images (Fig. 6). Blood metabolite-corrected RI values for the 40–60-min image frame were significantly reduced relative to control values by −61 ± 18% for PHEN ($p < 0.02$) and −66 ± 6% for HED ($p < 0.0006$) in desipramine-treated volunteers. Mean PHEN and HED reductions were not significantly different. Tracer retention was reduced uniformly throughout the myocardium. In only one volunteer was there a significant difference between the percent reductions of PHEN and HED (Volunteer 3, $p < 10^{-7}$). Representative time-activity curves of PHEN and HED are presented in Figure 7.

PHEN Washout Analysis

The myocardial washout of PHEN in normal volunteers was found to occur with an average half-time of 58.9 ± 5.2 min (range 51.7–68.9 min). Again, HED does not significantly clear

TABLE 1
Parameters for Intact Carbon-11-PHEN and Carbon-11-HED in Blood

	% Intact radiotracer = $A_1 \exp(-\lambda t) + C$		
	A_1 (%)	λ (min^{-1})	C (%)
PHEN (control, n = 12)	92.2 ± 5.8	0.0696 ± 0.0159	10.1 ± 3.7
PHEN (DMI block, n = 4)	88.6 ± 6.1	0.0805 ± 0.0166	11.1 ± 3.1
HED (control, n = 6)	100.3 ± 1.6	0.0240 ± 0.0025	0*
HED (DMI block, n = 4)	99.4 ± 1.2	0.0203 ± 0.0035	0*

*C was fixed at zero for exponential fitting of HED. p = NS for all comparisons between control and DMI block.
Values are mean ± s.d.

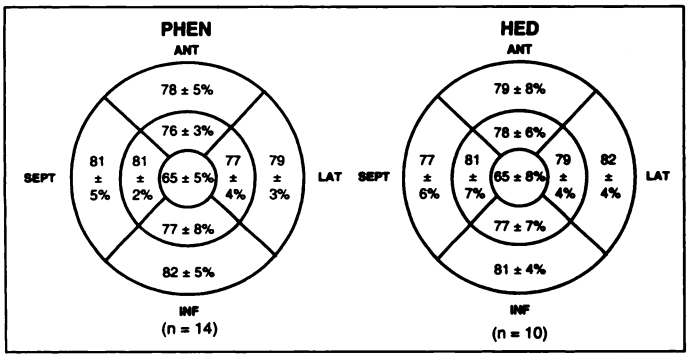

FIGURE 4. Polar maps of relative regional PHEN and HED distribution at 40–60 min in normal volunteers. For each volunteer, the polar map sector with the highest tissue retention of tracer was defined as 100%, and all other sectors normalized to this sector. Sectors were then averaged according to their regional location. These regional values were then averaged across all volunteers to calculate the population means and s.d. shown in the maps.

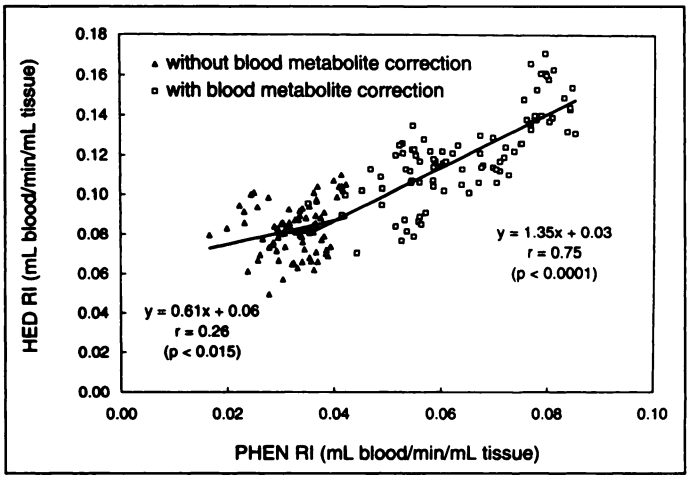

FIGURE 5. Correlation between PHEN and HED retention index (RI) values in normal volunteers. For each volunteer who had both PHEN and HED scans performed, regional average RI values for PHEN and HED are plotted against each other. RI values for 40–60-min image frame calculated with blood data uncorrected for metabolites (solid triangles) show a weak but significant correlation. When RI values are calculated with blood data corrected for metabolites (open squares) the correlation between PHEN and HED retention is stronger and highly significant.

from the heart, so it was not possible to estimate a washout half-time for this tracer.

DISCUSSION

Several studies with [^{123}I]*meta*-iodobenzylguanidine (MIBG) have demonstrated important changes in global and regional sympathetic function in patients with myocardial infarction (*19–22*), heart failure and cardiomyopathy (*23–27*) and peripheral neuropathy (*28*). A critique of clinical applications of MIBG has recently been published (*29*). The successful imaging of cardiac sympathetic neurons with MIBG using conventional scintigraphic imaging techniques and SPECT has encouraged the development of PET tracers of sympathetic neuronal function. The positron-emitting radionuclides ^{11}C and ^{18}F have been used in the synthesis of several norepinephrine analogs, including [^{11}C]HED (*1*), [^{11}C]epinephrine (*17*), 6-[^{18}F]fluoronorepinephrine (*30*), and 6-[^{18}F]fluorodopamine (*31, 32*). Heart image quality with these PET tracers in baboons (*33*) and humans (*4–6, 9, 34*) has generally been excellent with high specific neuronal uptake and improved target-to-background ratios. Studies with HED have demonstrated important changes in cardiac sympathetic innervation in patients with myocardial infarction (*5*), diabetic autonomic neuropathy (*6*), cardiac transplantation (*8*), and aborted sudden death (*7, 9*). Like MIBG, HED is not metabolized by monoamine oxidase (MAO) within the neuron. A norepinephrine analog such as PHEN which is susceptible to neuronal MAO metabolism might be an important investigative tool, permitting noninvasive assessments of autonomic function previously unavailable.

Phenylephrine (*m*-synephrine, neosynephrine) is a sympathomimetic drug used commonly as an over-the-counter nasal decongestant. In this study, we report the initial use of ^{11}C-labeled phenylephrine for imaging cardiac sympathetic innervation in normal volunteers. Tandem studies with HED were performed in a large subset of these volunteers. Neither radiopharmaceutical produced hemodynamic effects or other symptoms. The relative myocardial distributions of both tracers were very similar (Fig. 4). PHEN metabolites appeared in blood at approximately three times the rate of HED. This finding may be due to metabolism by MAO in MAO-rich tissues such as the liver, in addition to the heart. Importantly, PHEN clears from the normal myocardium with a mean half-time of 59 min, while HED levels in the heart remain constant. If the enhanced washout of PHEN from the heart proves to be related to neuronal MAO activity, regional examination of the washout half-times of PHEN in patients with various cardiac diseases may provide new insights into cardiac sympathetic integrity.

The faster clearance of PHEN from the heart leads to

TABLE 2
Regional Cardiac Retention Index (RI) Values* at 40–60 Minutes

	PHEN (n = 14)		HED (n = 10)	
Segments	Uncorrected blood data	Metabolite-corrected blood data	Uncorrected blood data	Metabolite-corrected blood data
Apical	0.0281 ± 0.0050	0.0544 ± 0.0131	0.070 ± 0.011	0.100 ± 0.018
Distal inferior	0.0334 ± 0.0071	0.0645 ± 0.0170	0.082 ± 0.012	0.118 ± 0.022
Distal lateral	0.0330 ± 0.0058	0.0635 ± 0.0141	0.084 ± 0.011	0.122 ± 0.022
Distal anterior	0.0328 ± 0.0051	0.0633 ± 0.0133	0.083 ± 0.014	0.121 ± 0.025
Distal septal	0.0348 ± 0.0054	0.0670 ± 0.0138	0.086 ± 0.012	0.124 ± 0.021
Proximal inferior	0.0351 ± 0.0057	0.0677 ± 0.0143	0.086 ± 0.011	0.125 ± 0.023
Proximal lateral	0.0339 ± 0.0050	0.0653 ± 0.0123	0.087 ± 0.009	0.126 ± 0.020
Proximal anterior	0.0336 ± 0.0048	0.0648 ± 0.0130	0.085 ± 0.014	0.123 ± 0.024
Proximal septal	0.0348 ± 0.0044	0.0669 ± 0.0115	0.082 ± 0.011	0.119 ± 0.019
Global averages	0.0325 ± 0.0052	0.0626 ± 0.0133	0.081 ± 0.011	0.117 ± 0.020

*Retention Index values have units of (ml blood/min/ml tissue).

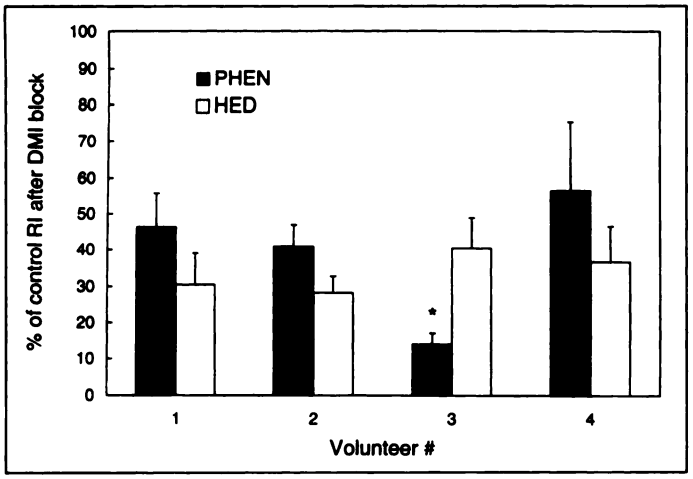

FIGURE 6. Effect of desipramine (DMI) pretreatment on retention of PHEN and HED. For each of the four volunteers, studied before and after oral administration of DMI, the mean RI value for the DMI study divided by the mean RI value of the corresponding control study are plotted, expressed as a percentage of control. RI values used were from the 40–60-min image frame, calculated using blood data corrected for metabolites. Error bars reflect the uncertainty in the percent reduction, calculated using the s.d. of the mean RI values. For Volunteer 3 only, PHEN retention was reduced significantly more than HED retention ($p < 10^{-7}$).

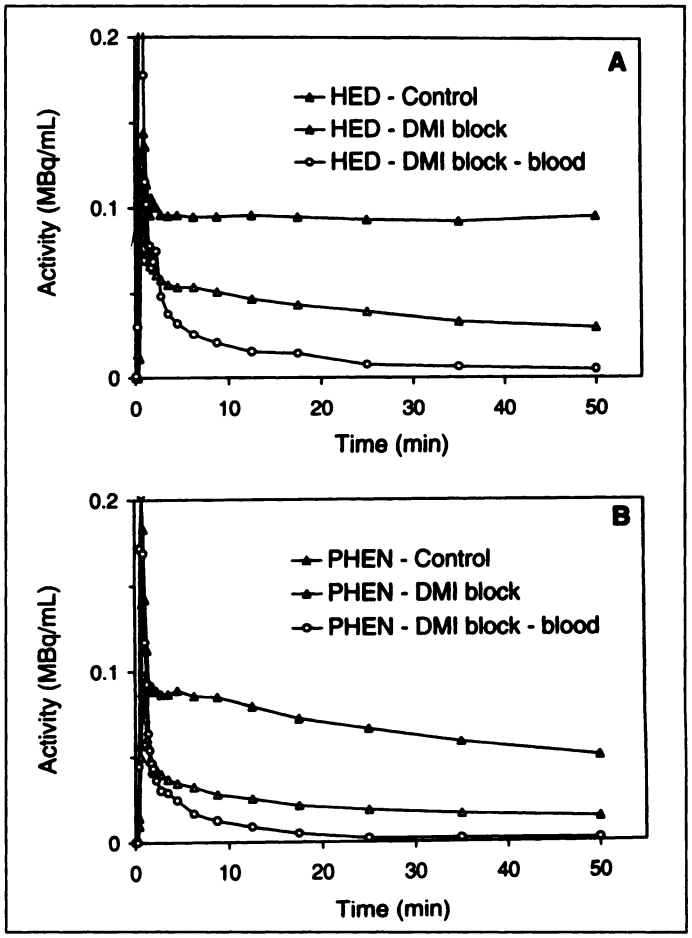

FIGURE 7. Effect of desipramine (DMI) on the myocardial kinetics of (A) HED and (B) PHEN. Representative time-activity curves from midventricular regions before and after oral administration of DMI are shown. Time-activity curves of intact tracer in blood from the DMI block studies are also plotted. All data are from the same normal volunteer shown in Figure 2. The pharmacologically induced reduction of neuronal norepinephrine transporters leads to a rapid disappearance of both PHEN and HED from the myocardium relative to controls.

retention index (RI) values for PHEN that are approximately half those of HED. When corrections for blood metabolites were made, the calculated RI values for PHEN and HED were significantly correlated. Clearly, myocardial levels of radiotracer are more dependent on the time course of intact tracer in the blood than on total blood radioactivity. Correcting the arterial blood data for metabolites is necessary to obtain an accurate blood-normalized measure of neuronal retention of tracer.

Apical concentrations of both PHEN and HED were lower than their respective concentrations in the remaining left ventricular regions (Table 2, Fig. 4). In studies in which regional tissue levels of norepinephrine in the left ventricles of dogs and primates have been directly measured, apical concentrations of norepinephrine have consistently been lower than those in the rest of the left ventricle (*35–39*). Studies of cardiac retention of radiolabeled catecholamines in dogs have demonstrated that apical uptake is significantly lower than other left ventricular regions (*36, 40*). Likewise, retention of [^{123}I]-*meta*-iodobenzylguanidine in normal human volunteers is lower in the apex than in the rest of the left ventricle (*28*). Together, these results strongly suggest that the density of cardiac sympathetic innervation in mammalian heart is significantly lower in the apex than in distal and proximal left ventricular regions.

The marked reduction in cardiac PHEN localization in the four normal subjects after oral desipramine (DMI) strongly suggests that PHEN primarily localizes in the sympathetic nerves of human heart. Blockade of the neuronal norepinephrine transporter with DMI has been used in rat (*41*), dog (Sherman PS and Wieland DM, *personal communication*, 1995), baboon (*33*) and man (*42–44*) to estimate the extent of neuronal localization of radiolabeled catecholamine analogs in the heart. In the same four human volunteers, DMI similarly decreased HED heart localization. The reduction in neuronal retention of PHEN and HED was uniform throughout the heart and occurred very early in the time course of the dynamic PET study (Fig. 7). The rapid early loss of tracer indicates that initial retention of PHEN and HED (i.e., tissue levels soon after blood levels have dropped dramatically, 3–5 min after tracer injection) is related to the number of available neuronal norepinephrine transporters at the time of tracer administration. After this initial neuronal uptake, subsequent kinetic behavior of the tracers will depend on all aspects of neuronal function, including neuronal transport, vesicular uptake and storage efficiency, neuronal firing rate and, for PHEN, neuronal MAO activity.

We did not evaluate larger doses of oral DMI, but it seems unlikely that the doses we used were sufficient to achieve a complete blockade of neuronal transporters (*45*). The residual heart levels of PHEN and HED seen in the DMI-block experiments are probably due to unblocked neuronal uptake. In in vivo rat studies, injection of DMI (10 mg/kg, i.p.) 30 min prior to intravenous injection of either HED or PHEN resulted in reductions of myocardial tracer retention at 60 min by 92% (*1*) and 77% (*12*), respectively. These reductions are higher than the mean percent reductions we observed in our DMI-block PET experiments. Also, these data suggest that PHEN has a somewhat lower neuronal selectivity than HED in the rat heart. Studies in isolated perfused rat hearts have shown that (–)-[^{3}H]phenylephrine is avidly transported by the extraneuronal norepinephrine transporter (uptake$_2$) (*46*), while accumulation of HED into the extraneuronal compartment is very low (*10*). Thus extraneuronal accumulation of PHEN may explain the lower reduction of PHEN retention relative to HED retention seen in rat hearts after blockade of neuronal transporters with DMI. However, these findings probably cannot be extrapolated

to the human heart. The rat heart is known to have a very active extraneuronal uptake system (*47*), while work by Dae and coworkers suggests that human heart, in contrast to rat and cat hearts, does not have an efficient extraneuronal uptake system (*48*).

Our usual paradigm has been to extensively evaluate radiotracers in animals before proceeding to human studies. Since phenylephrine is a common over-the-counter medication, we were able to obtain local permission to conduct PHEN studies in humans. We reasoned that if PHEN did not provide satisfactory images of the human myocardium or failed to efflux from the heart more rapidly than HED, extensive animal studies exploring the in vivo fate of PHEN ultimately would be of little clinical value. Before evaluation in humans, however, screening studies of PHEN in rats suggested that this tracer was a promising candidate for mapping heart neuronal MAO activity. After injection of either [^{3}H]phenylephrine or [^{11}C]phenylephrine, radioactivity selectively localized in the rat heart and subsequently washed out of the heart with a half-time of approximately 30 min (*12*). HED, in contrast, displayed a heart washout $T_{1/2}$ of >75 min. Sequestration of PHEN in the rat heart was blocked by DMI as well as by the vesicular transport blocker reserpine (*12–14*).

The literature on phenylephrine as a substrate for MAO is sparse, yet sufficient to prove that phenylephrine is deaminated by MAO. Pharmacokinetic studies of phenylephrine in humans found that the two deamination metabolites *m*-hydroxymandelic acid (HMA) and *m*-hydroxyphenylglycol (HOPEG) are major metabolites excreted in urine (*49, 50*). The *p*-isomer of phenylephrine, *p*-synephrine, has been demonstrated in vitro to be deaminated by both subtypes of MAO (MAO-A and MAO-B) using rat brain mitochondria (*51*). Related studies with *m*-octopamine (*52*) and *p*-octopamine (*53*), and *m*-tyramine and *p*-tyramine (*54*), indicate that such isomeric pairs have very similar MAO activity profiles, suggesting that *m*-synephrine (phenylephrine) is a substrate for both A and B forms of MAO. In what is perhaps the most relevant extant study, Rawlow and coworkers showed that (−)-[^{3}H]phenylephrine is metabolized by both the neuronal and extraneuronal pools of MAO in the isolated rat heart (*46*).

MAO cleaves PHEN at the α-carbon into two by-products: an unlabeled aldehyde and [^{11}C]methylamine. Methylamine (CH_3NH_2) is a freely diffusible molecule that should rapidly leave the neuron and enter the systemic circulation. Thus, in principle, the observed efflux rate of ^{11}C from the heart after initial uptake of PHEN contains information about the MAO activity in cardiac sympathetic neurons. Methylamine is not a substrate for MAO, but rather is metabolized by semicarbazide-sensitive amine oxidase (SSAO), which is found predominantly in vascular tissues and plasma (*55, 56*). Studies in which [^{14}C]methylamine was injected intravenously in rabbits indicate that a large fraction of the ^{14}C label was rapidly incorporated into $^{14}CO_2$, some of which was expired from the lungs, but with most being incorporated into [^{14}C]urea and [^{14}C]methylurea via the urea cycle (*57*).

Substitution of deuterium atoms for the two α-carbon hydrogen atoms slows the rate at which an MAO substrate is metabolized by MAO, since the bond energy of a carbon-deuterium bond is higher than that of a carbon-hydrogen bond (*58*). This deuterium isotope effect approach has often been used to slow the rate of MAO metabolism at the substrate level (*59–61*). We recently synthesized [^{11}C]-(−)-α,α-dideuterophenylephrine (D2-PHEN) to investigate the influence of MAO metabolism on the kinetics of PHEN (*62*). Studies with an isolated perfused rat heart preparation demonstrated that D2-PHEN cleared from the heart 1.8 times slower than PHEN (*13*). Also, when the isolated rat heart was infused with perfusate containing 100 μM of the MAO inhibitor pargyline for 30 min prior to PHEN administration, the kinetics of PHEN were identical to those of D2-PHEN. These results indicate that neuronal MAO activity significantly influences the efflux of radioactivity from the isolated rat heart after uptake of PHEN. We are currently performing PET studies of D2-PHEN in normal volunteers to assess the importance of neuronal MAO activity on the kinetics of PHEN in human heart.

These findings lay the groundwork for more detailed studies with PHEN in both humans and animals. The clinical potential of PHEN has yet to be established. However, since the uptake, retention and subsequent washout of PHEN depends on three different energy-requiring processes–neuronal transport, vesicular storage, neuronal MAO activity–this tracer may prove to be a more sensitive marker of overall neuronal function than HED. Furthermore, diseases may affect these three neuronal processes differently. For example, it has been suggested that myocardial ischemia affects principally heart neuronal MAO activity and vesicular storage (*63–65*). Heart failure, on the other hand, is characterized by reduced myocardial catecholamine stores (*66–69*). Some studies suggest that this may result from a defect in neuronal transport or vesicular storage, or both (*42, 70–72*), while others have found neuronal reuptake to be normal and attribute the increased norepinephrine spillover solely to increased sympathetic nerve firing (*73*). The involvement of the sympathetic nervous system in the progression of heart failure and the genesis of cardiac arrhythmias suggests the need for a sensitive, noninvasive metabolic marker of sympathetic neuronal function. Further tracer studies of the human heart will be aimed at determining the extent to which neuronal transport and vesicular storage, as well as neuronal MAO activity, can be quantified by the use of a single-injection PET study with PHEN.

CONCLUSION

PHEN, which can be synthesized with high specific activity and in tracer amounts sufficient for clinical studies, is completely free of hemodynamic or other side effects. PHEN images demonstrated excellent myocardial localization with image quality and uniformity of tracer distribution generally comparable to that of HED. PHEN clears from the myocardium with a measurable half-time while myocardial levels of HED remain constant, consistent with expected differences in the neuronal handling of these two radiotracers. These findings suggest that PHEN is a promising radiotracer for noninvasive assessment of cardiac sympathetic nerve function, using the same mechanisms of uptake, storage and metabolism that govern sympathetic neuronal handling of norepinephrine.

ACKNOWLEDGMENTS

We gratefully acknowledge the skilled assistance of the University of Michigan PET Technologists, Jill Rothley, Edward McKenna and Andrew Weeden. We also thank the Cyclotron/PET Chemistry staff for their reliable production of the radiotracers, especially Louis Tluczek and Steve Connor. We thank Patti Rose for her help in recruiting the volunteers and Linder Markham for her assistance in the preparation of this manuscript. This work was supported by grants #R01-HL47543 and #R01-HL27555 from the National Institutes of Health, Bethesda, MD.

REFERENCES

1. Rosenspire KC, Haka MS, Van Dort ME, et al. Synthesis and preliminary evaluation of carbon-11-meta-hydroxyephedrine: a false transmitter agent for heart neuronal imaging. *J Nucl Med* 1990;31:1328–1334.
2. DeGrado T, Hutchins G, Toorongian S, Wieland D, Schwaiger M. Myocardial kinetics

of carbon-11-meta-hydroxyephedrine: retention mechanisms and effects of norepinephrine. *J Nucl Med* 1993;34:1287–1293.
3. Wolpers HG, Nguyen N, Rosenspire K, Haka M, Wieland DM, Schwaiger M. ^{11}C-hydroxyephedrine as marker for neuronal catecholamine retention in reperfused canine myocardium. *Coronary Artery Disease* 1991;2:923–929.
4. Schwaiger M, Kalff V, Rosenspire K, et al. Noninvasive evaluation of sympathetic nervous system in human heart by positron emission tomography. *Circulation* 1990;82:457–464.
5. Allman KC, Wieland DM, Muzik O, Degrado TR, Wolfe ER, Schwaiger M. Carbon-11 hydroxyephedrine with positron emission tomography for serial assessment of cardiac adrenergic neuronal function after acute myocardial infarction in humans. *J Am Coll Cardiol* 1993;22:368–375.
6. Allman K, Stevens M, Wieland D, Wolfe E, Greene D, Schwaiger M. Noninvasive assessment of cardiac diabetic neuropathy by C-11 hydroxyephedrine and positron emission tomography. *J Am Coll Cardiol* 1993;22:1425–1432.
7. Calkins H, Allman K, Bolling S, et al. Correlation between scintigraphic evidence of regional sympathetic neuronal dysfunction and ventricular refractoriness in the human heart. *Circulation* 1993;88:172–179.
8. Schwaiger M, Hutchins G, Kalff V, et al. Evidence of regional catecholamine uptake and storage sites in the transplanted human heart by positron emission tomography. *J Clin Invest* 1991;87:1681–1690.
9. Calkins H, Lehmann M, Allman K, Schwaiger M. Scintigraphic pattern of regional cardiac sympathetic innervation in patients with familial long QT syndrome using positron emission tomography. *Circulation* 1993;87:1616–1621.
10. DeGrado TR, Toorongian SA, Hutchins GD, Wieland DM. Characterization of C-11 *m*-hydroxyephedrine (HED) kinetics in isolated rat heart [Abstract]. *J Nucl Med* 1992;33(suppl):870–871.
11. del Rosario R, Jung Y-W, Caraher J, et al. Carbon-11-phenylephrine. Marker for neuronal heart MAO [Abstract]. *J Nucl Med* 1994;35(suppl):7P.
12. del Rosario RB, Jung Y-W, Caraher J, Chakraborty PK, Sherman PS, Wieland DM. Synthesis and preliminary evaluation of [C-11] phenylephrine as a functional heart neuronal PET agent. *Nucl Med Biol* 1996;23:611–616.
13. Raffel DM, del Rosario RB, Tluczek L, Wieland DM. Kinetic properties of C-11 phenylephrine in isolated rat heart: effects of di-deuterium substitution, age, MAO inhibition, and reserpine [Abstract]. *J Nucl Med* 1995;36(suppl):90P.
14. Raffel DM, Corbett JR, Schwaiger M, Wieland DM. Mechanism-based strategies for mapping heart sympathetic nerve function. *Nucl Med Biol* 1995;22:1019–1026.
15. Khafagi F, Shapiro B, Fig L, Mallette S, Sisson J. Labetalol reduces iodine-131 MIBG uptake by pheochromocytoma and normal tissues. *J Nucl Med* 1989;30:481–489.
16. Jewett DM. A simple synthesis of [^{11}C]methyl triflate. *Appl Radiat Isot* 1992;43:1383–1385.
17. Chakraborty PK, Gildersleeve DL, Jewett DM, et al. High yield synthesis of high specific activity *R*-(−)-[^{11}C]epinephrine for routine PET studies in humans. *Nucl Med Biol* 1993;20:939–944.
18. Kotzerke J, Hicks RJ, Wolfe E, et al. Three-dimensional assessment of myocardial oxidative metabolism: a new approach for regional determination of PET-derived C-11 acetate kinetics. *J Nucl Med* 1990;31:1876–1893.
19. Kline RC, Swanson DP, Wieland DM, et al. Myocardial imaging in man with I-123-meta-iodobenzylguanidine. *J Nucl Med* 1981;22:129–132.
20. Dae M, Herre J, O'Connell J, Botvinick E, Newman D, Munoz L. Scintigraphic assessment of sympathetic innervation after transmural versus nontransmural myocardial infarction. *J Am Coll Cardiol* 1991;17:1416–1423.
21. Mantysarri M, Kuikka J, Hartikainen J, et al. Myocardial sympathetic nervous dysfunction detected with I-123-MIBG is associated with low heart rate variability after myocardial infarction. *J Nucl Med* 1995;36:956–961.
22. McGhie AI, Corbett JR, Akers MS, et al. Regional cardiac adrenergic function using I-123-meta-iodobenzylguanidine tomographic imaging after acute myocardial infarction. *Am J Cardiol* 1991;67:236–242.
23. Henderson EB, Kahn JK, Corbett JR, et al. Abnormal I-123-metaiodobenzylguanidine myocardial washout and distribution may reflect myocardial adrenergic derangement in patients with congestive cardiomyopathy. *Circulation* 1988;78:1192–1199.
24. Schofer J, Speilmann R, Schuchert A, Weber K, Schlüter M. Iodine-123-meta-iodobenzylguanidine scintigraphy: a noninvasive method to demonstrate myocardial adrenergic nervous system disintegrity in patients with idiopathic dilated cardiomyopathy. *J Am Coll Cardiol* 1988;12:1252–1258.
25. Glowniak J, Turner F, Gray L, Palac R, Lagunas-Solar M, Woodward W. Iodine-123 metaiodobenzylguanidine imaging of the heart in idiopathic congestive cardiomyopathy and cardiac transplants. *J Nucl Med* 1989;30:1182–1191.
26. Merlet P, Valette H, Dubois-Randé J-L, et al. Prognostic value of cardiac metaiodobenzylguanidine imaging in patients with heart failure. *J Nucl Med* 1992;33:471–477.
27. Rabinovitch MA, Rose CP, Schwab AJ, et al. A method of dynamic analysis of iodine-123-meta-iodobenzylguanidine scintigrams in cardiac mechanical overload hypertrophy and failure. *J Nucl Med* 1993;34:589–600.
28. Sisson J, Shapiro B, Meyers L, et al. Metaiodobenzylguanidine to map scintigraphically the adrenergic nervous system in man. *J Nucl Med* 1987;28:1625–1636.
29. Glowniak JV. Cardiac studies with metaiodobenzylguanidine: a critique of methods and interpretation of results. *J Nucl Med* 1995;36:2133–2137.
30. Ding Y-S, Fowler J, Gatley S, Dewey S, Wolf A. Synthesis of high specific activity (+) and (−) 6-[^{18}F]fluoronorepinephrine via the nucleophilic aromatic substitution reaction. *J Med Chem* 1991;34:767–771.
31. Eisenhofer G, Hovevey-Sion D, Kopin IJ, et al. Neuronal uptake and metabolism of 2- and 6-fluorodopamine: false neurotransmitters for positron emission tomographic imaging of sympathetically innervated tissues. *J Pharmacol Exper Ther* 1989;248:419–427.
32. Ding Y-S, Fowler JS, Gatley S, Dewey S, Wolf A, Schlyer D. Synthesis of high specific activity (+) and (−) 6-[^{18}F]fluorodopamine for PET studies of sympathetic nervous tissue. *J Med Chem* 1991;34:861–863.
33. Ding Y-S, Fowler JS, Dewey SL, et al. Comparison of high specific activity (−) and (+)-6-[F-18]fluoronorepinephrine and 6-[F-18]fluorodopamine in baboons: heart uptake, metabolism and the effect of desipramine. *J Nucl Med* 1993;34:619–629.
34. Schwaiger M, Wieland D, Muzik O, et al. Comparison of C-11-epinephrine and C-11 HED for evaluation of sympathetic neurons of the heart [Abstract]. *J Nucl Med* 1993;34(suppl):13P.
35. Pierpont G, DeMaster E, Reynolds S, Cohn J. Ventricular myocardial catecholamines in primates. *J Lab Clin Med* 1985;106:205–210.
36. Pierpont G, Cohn J, DeMaster E. Regional differences in adrenergic function within the left ventricle. *Am J Physiol* 1984;246:H824–H829.
37. Kaye MP, Tyce GM. Norepinephrine uptake as an indicator of cardiac reinnervation in dogs. *Am J Physiol* 1978;235:H289–H294.
38. Mathes P, Gudbjarnason S. Changes in norepinephrine stores in the canine heart following experimental myocardial infarction. *Am Heart J* 1971;81:211–219.
39. Angelakos ET. Regional distribution of catecholamines in the dog heart. *Circ Res* 1965;16:39–44.
40. Chilian W, Boatwright R, Shoji T, Griggs DJ. Regional uptake of [^{3}H]-norepinephrine by the canine left ventricle. *Proc Soc Exp Biol Med* 1982;171:158–163.
41. Wieland DM, Rosenspire KC, Hutchins GD, et al. Neuronal mapping of the heart with 6-[^{18}F]fluorometaraminol. *J Med Chem* 1990;33:956–964.
42. Goldstein D, Brush J Jr, Eisenhofer G, Stull R, Esler M. In vivo measurement of neuronal uptake of norepinephrine in the human heart. *Circulation* 1988;78:41–48.
43. Esler MD, Wallin G, Dorward PK, et al. Effects of desipramine on sympathetic nerve firing and norepinephrine spillover to plasma in humans. *Am J Physiol* 1991;260:R817–R823.
44. Eisenhofer G, Esler MD, Meredith IT, Ferrier C, Lambert G, Jennings G. Neuronal re-uptake of noradrenaline by sympathetic nerves in humans. *Clin Science* 1991;80:257–263.
45. Esler M. Clinical application of the noradrenaline spillover methodology: delineation of regional human sympathetic nervous responses. *Pharmacol Toxicol* 1993;73:243–253.
46. Rawlow A, Fleig H, Kurahashi K, Trendelenburg. The neuronal and extraneuronal uptake and deamination of [H-3]-(−)-phenylephrine in the perfused rat heart. *Arch Pharmacol* 1980;314:237–247.
47. Trendelenburg U. The extraneuronal uptake and metabolism of catecholamines. In: Weiner N, ed. *Catecholamines I: handbook of experimental pharmacology, vol. 90/I.* Berlin, Germany: Springer-Verlag; 1988:281–319.
48. Dae MW, De Marco T, Botvinick EH, et al. Scintigraphic assessment of MIBG uptake in globally denervated human and canine hearts—implications for clinical studies. *J Nucl Med* 1992;33:1444–1450.
49. Ibrahim KE, Midgley JM, Crowley JR, Williams CM. The mammalian metabolism of *R*-(−)-*m*-synephrine. *J Pharm Pharmacol* 1983;35:144–147.
50. Hengstmann JH, Goronzy J. Pharmacokinetics of H3-phenylephrine in man. *Eur J Clin Pharmacol* 1982;21:335–341.
51. Suzuki O, Matsumoto T, Oya M, Katsumata Y. Oxidation of synephrine by type A and type B monoamine oxidase. *Experientia* 1979;35:1283–1284.
52. Suzuki O, Hattori H. *m*-Octopamine as a substrate for monoamine oxidase. *Life Sci* 1979;25:1231–1236.
53. Suzuki O, Katsumata Y, Oya M. Oxidation of phenylethanolamine and octopamine by type A and type B monoamine oxidase: effect of substrate concentration. *Biochem Pharmac* 1979;28:2327–2332.
54. Suzuki O, Oya M, Katsumata Y. Oxidation of *p*-, *m*- and *o*-tyramine by type A and type B monoamine oxidase. *Biochem Pharmacol* 1979;28:2682–2684.
55. Lyles G, Holt A, Marshall C. Further studies on the metabolism of methylamine by semicarbazide-sensitive amine oxidase activities in human plasma, umbilical artery and rat aorta. *J Pharm Pharmacol* 1990:332–338.
56. Boor PJ, Trent MB, Lyles GA, Tao M, Ansari GA. Methylamine metabolism to formaldehyde by vascular semicarbazide-sensitive amine oxidase. *Toxicology* 1992;73:251–258.
57. Dar M, Bowman E. In vivo mammalian metabolism of methylamine and methylurea and their metabolic interrelationship. *Drug Metab Dispos Biol Fate Chem* 1985;13(6):682–689.
58. March J. *Advanced organic chemistry,* 4th ed. New York, NY: John Wiley & Sons; 1992.
59. Yu PH, Bailey BA, Durden DA, Boulton AA. Stereospecific deuterium substitution at the α-carbon position of dopamine and its effects on oxidative deamination catalyzed by MAO-A and MAO-B from different tissues. *Biochem Pharmacol* 1986;35:1027–1036.
60. Tominaga T, Inoue O, Suzuki K, Yamasaki T, Hirobe M. Nitrogen-13-β-Phenethylamine ([N-13]PEA). A prototype tracer for measurement of MAO-B activity in heart. *Biochem Pharmacol* 1987;36:3671–3675.
61. Ding Y-S, Fowler JS, Gatley SJ, Logan J, Volkow ND, Shea C. Mechanistic positron emission tomography studies of 6-[^{18}F]fluorodopamine in living baboon heart: selective imaging and control of radiotracer metabolism using the deuterium isotope effect. *J Neurochem* 1995;65:682–690.
62. del Rosario RB, Wieland DM. Synthesis of [^{11}C](−)-α-α-dideutero-phenylephrine for in vivo kinetic isotope studies. *J Lab Compd Radiopharm* 1995;36:625–630.
63. Bajusz E, Jasmin G. Histochemical studies on the myocardium following experimental interference with coronary circulation in the rat. I. Occlusion of coronary artery. *Acta Histochem* 1964;18:222–237.
64. Bajusz E, Jasmin G. Observations on histochemical differential diagnosis between primary and secondary cardiomyopathies: behavior of monoamine oxidase, phosphorylase, and glycogen in heart muscle. *Am Heart J* 1965;69:83–92.
65. Schömig A, Kurz T, Richardt G, Schömig E. Neuronal sodium homeostasis and axoplasmic amine concentration determine calcium-independent noradrenaline release in normoxic and ischemic rat heart. *Circ Res* 1988;63:214–226.
66. Chidsey CA, Braunwald E, Morrow AG, Mason DT. Myocardial norepinephrine concentration in man. Effects of reserpine and of congestive heart failure. *N Engl J Med* 1963;269:653–659.

67. Pentillä O, Kyösola K, Partanen S, Merikallio E, Siltanen P. Studies of auricular catecholamines by fluorescence histochemistry in various heart diseases of man. *Virchows Arch A Pathol Pathol Anat* 1977;373:279–292.
68. Borchard F, ed. The adrenergic nerves of the normal and the hypertrophied heart. In: Bargmann W, Doerr W, eds. *Normal and pathological anatomy, vol. 33.* Stuttgart, Germany: Georg Thieme; 1978.
69. Kawai C, Yui Y, Hoshino T, Sasayama S, Matsumori A. Myocardial catecholamines in hypertrophic and dilated (congestive) cardiomyopathy: a biopsy study. *J Am Coll Cardiol* 1983;2:834–840.
70. Rose CP, Burgess JH, Cousineau D. Tracer norepinephrine kinetics in coronary circulation of patients with heart failure secondary to chronic pressure and volume overload. *J Clin Invest* 1985;76:1740–1747.
71. Böhm M, La Roseé K, Schwinger RHG, Erdmann E. Evidence for reduction of norepinephrine uptake sites in the failing human heart. *J Am Coll Cardiol* 1995;25: 146–153.
72. Sole M, Helke C, Jacobowitz D. Increased dopamine in the failing hamster heart: transvesicular transport of dopamine limits the rate of norepinephrine synthesis. *Am J Cardiol* 1982;49:1682–1690.
73. Meredith I, Eisenhofer G, Lambert G, Dewar E, Jennings G, Esler M. Cardiac sympathetic nervous activity in congestive heart failure: evidence for increased neuronal norepinephrine release and preserved neuronal uptake. *Circulation* 1993;88: 136–145.

Dopamine D2 Receptor Imaging in Pituitary Adenomas Using Iodine-123-Epidepride and SPECT

Walter Pirker, Michaela Riedl, Anton Luger, Thomas Czech, Karl Rössler, Susanne Asenbaum, Peter Angelberger, Johannes Kornhuber, Lüder Deecke, Ivo Podreka and Thomas Brücke

University Clinics for Neurology and Nuclear Medicine, Internal Medicine III, Neurosurgery, Vienna; and Forschungszentrum Seibersdorf, Austria Department of Psychiatry, University of Würzburg, Federal Republic of Germany

Epidepride is a novel benzamide derivative with high affinity for D2 receptors. Epidepride, in its ^{123}I-labeled form, can be used for SPECT imaging of striatal and extrastriatal dopamine D2 receptors. The present study evaluated the usefulness of epidepride and SPECT for in vivo imaging of dopamine receptors in pituitary adenomas. **Methods:** SPECT imaging was performed in 19 patients with pituitary adenomas (among them 9 patients had prolactinoma, 4 acromegaly, 4 clinically nonfunctioning pituitary adenoma, 1 Cushing's disease and 1 Nelson's syndrome) and 7 control subjects 180 min after intravenous bolus injection of 3.9 ± 1.1 mCi [^{123}I]epidepride. The ratio target/cerebellum minus 1, reflecting specific/nonspecific binding was used as semiquantitative measure of D2 receptor binding. **Results:** Eight of nine prolactinoma patients demonstrated specific binding within the adenoma. The adenoma/cerebellum ratio 3 hr p.i. showed a wide variation with values from 2.5–33. In three prolactinomas, binding was higher than in the striatum. Specific binding within the lower range of prolactinomas (adenoma/cerebellum ratios 2 and 4.8) could be demonstrated in two of four GH-secreting adenomas. All four nonfunctioning tumors showed specific binding. The adenoma/cerebellum ratio was within the lower range of prolactinomas (5.2–7.5) in three of these patients but extremely high in one (52.3). No specific tracer uptake could be demonstrated in patients with Cushing's disease or Nelson's syndrome. The striatum/cerebellum ratio 3 hr p.i. in pituitary adenoma patients was not significantly different from control subjects (17.3 ± 5.5 versus 17.8 ± 6.6; patients versus control subjects). **Conclusion:** Epidepride appears to be an excellent ligand for in vivo imaging of dopamine D2 receptors in pituitary adenomas. Epidepride SPECT could serve as a predictor for response to dopamine agonist treatment.

Key Words: dopamine; D2 receptors; epidepride; SPECT; pituitary adenomas

J Nucl Med 1996; 37:1931–1937

Pituitary adenomas are relatively common, amounting to about 5%-10% of all intracranial tumors. The majority of pituitary adenomas is characterized by hormonal secretion. Therefore, these tumors result in well-known clinical syndromes such as acromegaly or Cushing's disease. About 30% of pituitary adenomas secrete either none or a relatively low amount of hormone, or a hormone that does not produce a recognizable clinical syndrome. The latter adenomas are referred to as "clinically nonfunctioning" pituitary adenomas (*1*).

Membrane binding studies have identified dopamine receptors in normal anterior pituitary (*2–4*) as well as in prolactinomas (*2–6*), GH-secreting pituitary adenomas (*2,5,7,8*) and clinically nonfunctioning pituitary adenomas (*4,5,8*). The dopamine receptors in the normal anterior pituitary and in pituitary adenomas are of D2 subtype (*9*). The presence of dopamine receptors in pituitary adenomas is the pharmacological basis for the treatment of these tumors with dopamine agonists. Ergot-derived substances like bromocriptine, lisuride and cabergoline and recently the nonergot dopamine agonist quinagolide (CV 205–502) are widely used for the medical treatment of prolactinomas and occasionally tried in GH-secreting adenomas.

Bromocriptine treatment leads to a clear-cut reduction of tumor size in about 60% of prolactinomas and to a reduction or normalization of prolactin (PRL) secretion in most but not all prolactinoma patients (*6,10*). In acromegaly, dopamine agonist treatment lowers plasma GH levels in 50% of patients, but normalization of plasma IGF-I, which may be a more appropriate measure of clinical efficacy, is achieved only in 10% of patients. A reduction of tumor size is observed only in a minority of patients (*11*). However, symptomatic improvement is observed in a large percentage of acromegalic patients during dopamine agonist treatment, even though GH levels are not adequately suppressed (*11*). Until recently, medical treatment played a minor role in clinically nonfunctioning pituitary adenomas, but decreased tumor size, as reported by Kwekkeboom et al. (*12*), necessitated medical treatment for several patients undergoing dopamine agonist treatment.

Dopamine agonist sensitive and resistant adenoma patients are clinically indistinguishable. No reliable laboratory test is known that may predict response to dopaminergic treatment (*6,11*). Using membrane binding techniques it was shown in prolactinomas that the density of D2 receptors is markedly reduced in bromocriptine resistant adenomas as compared to dopamine agonist sensitive adenomas (*6*).

Muhr et al. (*13,14*) and Bergström et al. (*15*) who pioneered PET imaging of pituitary adenomas used ^{11}C-labeled raclopride

Received Nov. 28, 1995; revision accepted Apr. 4, 1996.
For correspondence or reprints contact: Walter Pirker, MD, Neurologische Universitätsklinik, Währiger Gürtel 18–20, A-1090 Wien, Austria.